

# Synthesis of Crown Ether End-Capped PM6 Copolymers with Tunable Molecular Weight for Organic Solar Cells

Yiming Li, Jiaqing Liu, Ke Shui, Fan Xie, Xuan Li, Yi Lin, Zehua Zhou, Qing Zhang, Fengqi Guo, Lijun Li,\* Jinchong Xiao,\* Meng Wang,\* and Chang-Qi Ma\*



Cite This: *Macromolecules* 2023, 56, 6276–6289



Read Online

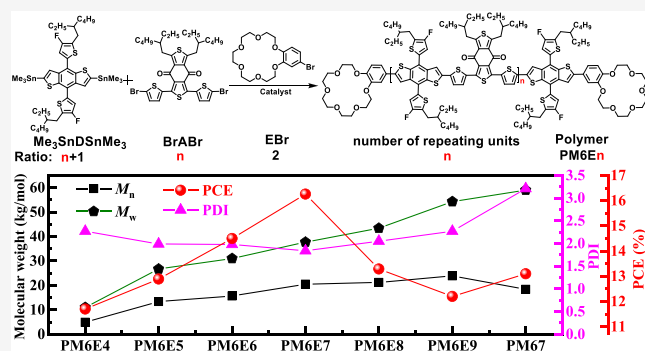
ACCESS |

Metrics & More

Article Recommendations

Supporting Information

**ABSTRACT:** Poly-[(2,6-(4,8-bis(5-(2-ethylhexyl-3-fluoro)-thiophen-2-yl)-benzo[1,2-*b*:4,5-*b'*]-dithiophene))-*alt*-(5,5-(1',3'-di-2-thienyl-5',7'-bis(2-ethylhexyl)benzo[1',2'-*c*:4',5'-*c'*]-dithiophene-4,8-dione))] (PM6) is one of the star molecules in organic solar cells (OSCs). However, PM6 has been suffering from molecular weight control and unreacted terminal groups. Thus, synthesizing high-quality polymers without batch-to-batch variations has been challenging for many years. Herein, a one-step protocol of both end-capping and polymerization at the same time was developed to prepare end-capped PM6 with molecular weight controlled by changing the monomer ratio. Specifically, non-end-capped PM67 and a series of PM6En with different molecular weights were synthesized and characterized. Our research findings indicated that (1) these copolymers' number-average molecular weights ( $M_n$ s) and weight-average molecular weights ( $M_w$ s) were measured to be almost linearly increased. Although textbooks have mentioned the nonequivalent ratio monomer strategy to regulate the molecular weight of polymers, the end-capping yield has not been reported in the research of OSCs due to a lack of efficient experiments and instruments to measure the low percentage of end groups in the polymer. (2) Since the selected end-capping reagent 4'-bromobenzo-18-crown-6 (EBr) can be easily distinguished from the PM6 main backbone, we first measured the end-capping yield by both nuclear magnetic resonance (NMR) and matrix-assisted laser desorption/ionization time-of-flight mass spectra (MALDI-TOF-MS). We applied this approach for the first time to synthesize polymers with reasonable end-capping yields (40–97%) for OSCs. (3) Surprisingly, 18-crown-6 can reduce end-group defects, lower the polydispersity index (PDI) of the polymer, and achieve suitable morphology and mobility. As a result, the end-capped PM6E7-based device exhibited the best stability and power conversion efficiency (PCE) compared to those of the other end-capped or non-end-capped polymers. Both the end groups and molecular weight significantly affect the performance of the OSCs. PM6 and other copolymers could be finely tuned by subtly changing the molecular weights or end-cap groups with functional building blocks. Our research will stimulate the development of OSCs and other applications of copolymers.



## 1. INTRODUCTION

Organic solar cells (OSCs) can be flexible, lightweight, colorful, and large-area printing, which attracted extensive attention to increase their photovoltaic performance.<sup>1,2</sup> Owing to the development of new materials and device fabrication skills, the best power conversion efficiency (PCE) of single-junction and tandem OSCs have reached over 19%<sup>3–8</sup> and 20%,<sup>9</sup> respectively. Generally, OSCs are based on a bulk heterojunction (BHJ) structure formed by a donor–acceptor (D–A) copolymer and small molecule acceptor.<sup>10–12</sup> Both the molecular weight and stability of the polymer are vital to determine the photovoltaic performance.<sup>13–16</sup> But the conjugated polymers have suffered from batch-to-batch variations, which may be caused by molecular weight control and unreacted end traps.<sup>17–22</sup> Nowadays, most of the polymers for OSCs are synthesized by Stille coupling, but the remaining

terminal groups (unreacted halogen, trimethyltin, or by-products) will be left if the polymer has not been end-capped efficiently.<sup>23–27</sup> These end sites would disturb the molecular packing,<sup>28</sup> capture charge carriers,<sup>29</sup> induce bad morphology,<sup>30</sup> decrease the crystallinity,<sup>31</sup> and result in poor mobility.<sup>30</sup> For instance, Huo et al. decreased the bromine atom percentage by end-capping Soxhlet-purified PM6, which had significant improvement on the photovoltaic performance of non-fullerene solar cells.<sup>23</sup> Zhou et al. employed a two-step end-

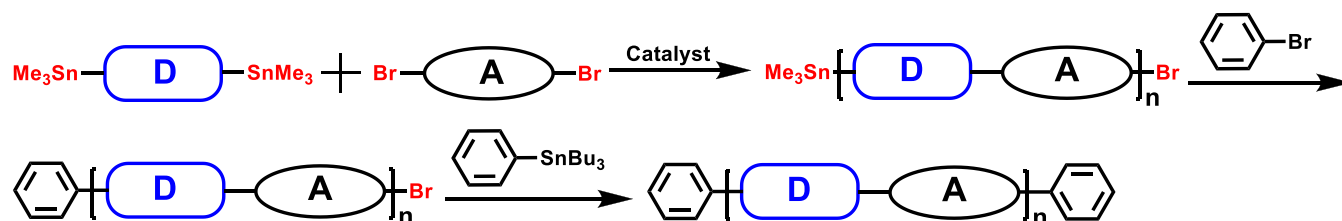
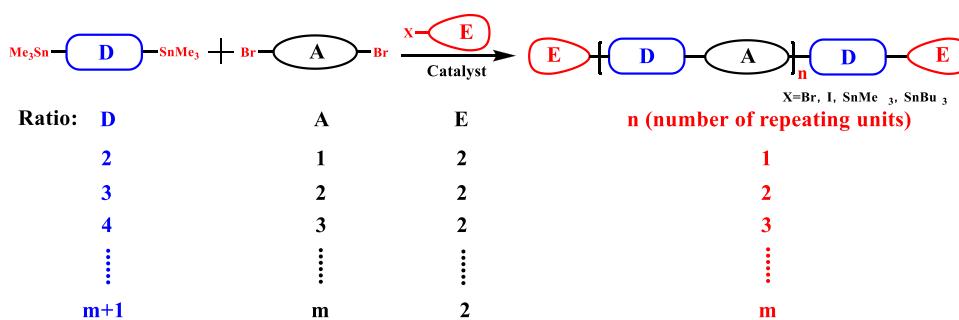
Received: April 25, 2023

Revised: June 26, 2023

Published: July 31, 2023



Scheme 1. Synthesis of the D–A Copolymer and Two-Step End-Capped Polymer

Scheme 2. Synthesis of Donor-Excessed E(DA)<sub>n</sub>DE

capping reaction right after polymerization to achieve the active layer film with optimized molecular orientation, morphology, and reduced nonradiative energy loss, resulting in improvement of both efficiency and stability for non-fullerene OSCs.<sup>32</sup>

End-capping is one of the simple but efficient ways to improve stability and device performance.<sup>23,33–36</sup> Classically, two-step end-capping was applied using two excessive benzene (or thiophene) derivatives to protect the two end sites (Scheme 1).<sup>37,38</sup> Obviously, this two-step method would cost much time, which could increase the possibility of side reactions such as destannylation, debromination, and homocoupling.<sup>18,39–41</sup> This method will not only reduce the yield of polymerization but also lead to bad photovoltaic performance.<sup>40,41</sup> Besides, compared with the backbone and side chains of conjugated copolymers, the end-capping sites generally occupied a tiny amount, and have been difficult to study the end-capping yield in depth.<sup>23,33</sup>

It is tricky to monitor the Stille polycondensation process and control the molecular weight as demanded.<sup>19,42</sup> Stopping the polymerization at the right time is the most easily proposed solution to achieve suitable molecular weight<sup>22,43</sup> but often requires a skilled chemist to perform several careful experiments to minimize operational error.<sup>22,42</sup> Many factors such as a different person, time, or batch of starting materials will make polymerization out of control. Thus, controlling time does not work very well all of the time.<sup>22,44</sup> Hence, the molecular weight can be roughly controlled to some extent by strictly adjusting the Stille coupling time while keeping other parameters unchanged.<sup>18</sup> The preparation of PM6 has already been so complicated that controlling the molecular weight and end-capping the polymer at the same time is much more challenging.<sup>19,43,45</sup>

Li et al. reported that incorporating more D units into the alternate D–A polymer backbone could finely tune the photovoltaic properties of the copolymers.<sup>46</sup> There is also much research about changing the monomer ratio to control the molecular weight of polymers synthesized by the Passerini reaction,<sup>47</sup> aqueous free-radical copolymerization,<sup>48</sup> and ring-opening metathesis polymerization.<sup>49</sup> Koldemir et al. reported

a simple one-pot end-capping polymerization by a 1% stoichiometric imbalance of the difunctional monomers. Relatively high-activity 1-iodo-4-methylbenzene was chosen as the end-capping reagent and added after the nonequivalent polymerization had reacted for 78 h to ensure sufficient polymerization and end-capping functionality.<sup>30</sup> Inspired by these results, we proposed combining a nonequivalent D–A ratio with a functional molecule to synthesize end-capped copolymers with tunable molecular weight in one pot. A low-activity end-capping reagent and mild conditions (low-activity catalyst and temperature gradients) were also used to increase the chemoselectivity between the polymerization and end-capping reaction. We expect the mixture to polymerize in the beginning and end-capping in the end to ensure a high yield. Theoretically, the molecular weight can also be controlled by changing the ratio between donor and acceptor monomers at the same time. A standard protocol of the end-capped polymer was developed and used to synthesize a series of PM6En by changing the D/A ratio. Their molecular weights were approximately linearly increasing as the theoretical repeating unit numbers (*n*) grew. This novel and effective nonequivalent D–A end-capping polymerization strategy proposed in this work would not only simplify the polymer synthesis efficiently but also pave the way for large-scale synthesis.

## 2. RESULTS AND DISCUSSION

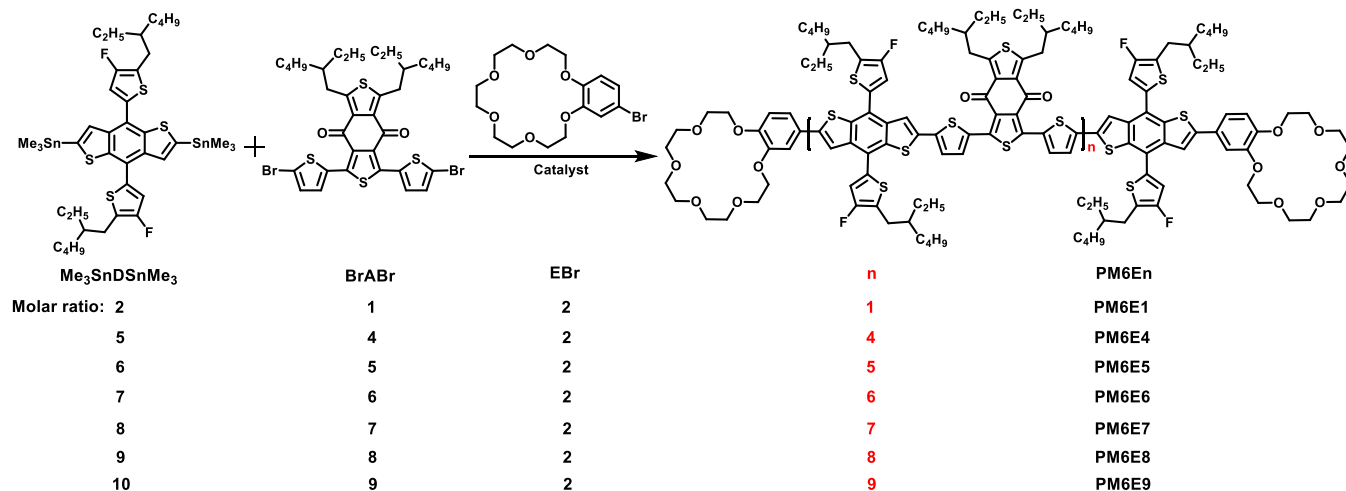
**2.1. Polymer Synthesis and Characterization.** As shown in textbooks,<sup>50–52</sup> a Stille coupling-prepared copolymer should satisfy eq 1

$$\bar{X}_n = 2n + 1 = (1 + r)/(1 + r - 2rp) \quad (1)$$

where  $\bar{X}_n$ , *n*, *r*, and *p* represent the degree of polymerization, the number of repeating units, the ratio between two D–A monomers (*r* ≤ 1), and the degree of reaction, respectively.

For a specific reaction, *p* should be almost constant. Thus, it is possible to control the polymer molecular weight by tuning *r* in theory, as shown in eq 2

## Scheme 3. Synthesis of PM6En



$$M_{\text{Polymer}} = M_{\text{End groups}} + nM_{\text{Repeat unit}}$$

$$= M_{\text{End groups}} + pM_{\text{Repeat unit}} / (1/r - 2p + 1) \quad (2)$$

where  $M_{\text{Polymer}}$ ,  $M_{\text{Repeat unit}}$ , and  $M_{\text{End groups}}$  represent the molecular weights of the polymer, repeat unit, and end groups, respectively.

Theoretically, an equivalent D–A ratio ( $r = 1$ ) could synthesize polymers with few end groups, especially when the molecular weight is high enough. But, the nonequivalent D–A ratio ( $r \neq 1$ ) will yield polymers with much more unreacted groups than normal, which may lead to bad stability and PCE. Here, we proposed to end-cap and control the molecular weight of the target polymer at the same time. As shown in Scheme 2, if the starting materials converted to the polymer completely,  $n$  should be 1 when the molecular number of  $N_{\text{Donor}}$ ,  $N_{\text{Acceptor}}$ , and  $N_{\text{End-capping reagent}}$  was fixed to 2, 1, and 2, respectively. Similarly, changing the ratio to  $(m + 1):m:2$  could obtain a polymer with  $n = m$ . Thus, based on the high yield of palladium-catalyzed Stille coupling, it is possible to control the polymer molecular weight by tuning the  $N_{\text{Donor}}/N_{\text{Acceptor}}$  ratio theoretically.<sup>23,53,54</sup> If the reaction speed difference between the end-capping and polymerization is not big enough, the end-capping reaction will occur at the beginning of the reaction and yield end-capped donor or acceptor monomer derivatives with low molecular weights.<sup>36</sup> To avoid this problem, the first choice is to increase the activation energy offset between these two reactions. Second, mild reaction conditions are used to enhance the chemoselectivity.

As shown in Scheme 3, we proposed to enhance the reaction energy barrier difference between the polycondensation and end-capping reaction by choosing a less reactive end-capping reagent (EBr), mild catalyst  $[\text{Pd}(\text{PPh}_3)_4]$ , and gradient heating. Only in this way will the mixture mainly polymerize at first and end-cap at last to obtain desired polymers with specific molecular weight in reasonably high yields. PM6En were synthesized by the palladium-catalyzed Stille polycondensation among monomer 4,8-bis(5-(2-ethylhexyl)-4-fluorothiophen-2-yl)(benzo[1,2-*b*:4,5-*b'*])dithiophene-2,6-diyl)bis(trimethylstannane) ( $\text{Me}_3\text{SnDSnMe}_3$ ), 1,3-bis(5-bromothiophen-2-yl)-5,7-bis(2-ethylhexyl)-4*H*,8*H*-benzo[1,2-*c*:4,5-*c'*]-dithiophene-4,8-dione (BrABr), and EBr (Scheme 3). Commercially available EBr was chosen as the end-capping

reagent due to it being effectively distinguished by NMR and MALDI-TOF-MS from the polymer backbone and alkyl side chains.

The copolymer is composed of a series of molecules with different molecular weights. Compared to a low-molecular-weight polymer, it is much more difficult to analyze a higher-molecular-weight copolymer by MALDI-TOF-MS and NMR due to low solubility and many repeating units. The high-molecular-weight molecules were generally underestimated by MALDI-TOF-MS and NMR. To evaluate the end-capping effect clearly by MALDI-TOF-MS and NMR, the low-molecular-weight PM6E1 and PM61 were synthesized by fixing the D/A/E ratio to 2:1:2 and 2:1:0, respectively. MALDI-TOF-MS was performed to measure the target molecules, with the results and corresponding structures plotted in Figure 1a.

The molecular weights of DA, D, A, and E units are 1222, 613, 607, and 311 g/mol, respectively. The spectrum should exhibit typical polymer characters that the peak with an  $m/z$  value of  $x + 1222N$  ( $N$  is a positive integer) corresponded to a structure with  $N$  repeating units more than the peak at  $x$ . It should be noted that many of these chemical structures were methyl end-capped or formed by homocoupling between two  $\text{Me}_3\text{Sn}$ -containing molecules in these curves, which had already been reported in other reports.<sup>18,55–58</sup> Interestingly, homocoupling of  $\text{Me}_3\text{SnDSnMe}_3$  were found in both PM6E1 and PM61. Compared with PM61, PM6E1 exhibited a lower homocoupling ratio, a smaller full-width at half maximum, and fewer peaks, especially when the  $m/z$  value was below 1200. These features proved that the end-capping reagent EBr could react efficiently with  $\text{Me}_3\text{Sn}$  in high yield and hence reduce the chance of side reactions. Considering the high molecular weight bias by MALDI-TOF-MS, the so-called “polydispersity index (PDI)” of PM6E1 should be much smaller than PM61, and the yield of EDAAE was much higher than DADMe<sub>2</sub> according to Figure 1a.<sup>23,59</sup>

The yield of end-capping by E estimated from MALDI-TOF-MS ( $Y_{\text{MALDI}}$ ) and NMR ( $Y_{\text{NMR}}$ ) was summarized in Table 1. It should be noted that the end-capping yields are rarely mentioned due to the end-capping being low percentage and difficult to measure accurately. Here, EBr was used as the end-capping reagent to calculate the end-capping yield by both MALDI-TOF-MS and NMR to enhance the reliability of test results. The low-molecular-weight PM61 and PM6E1 exhibited

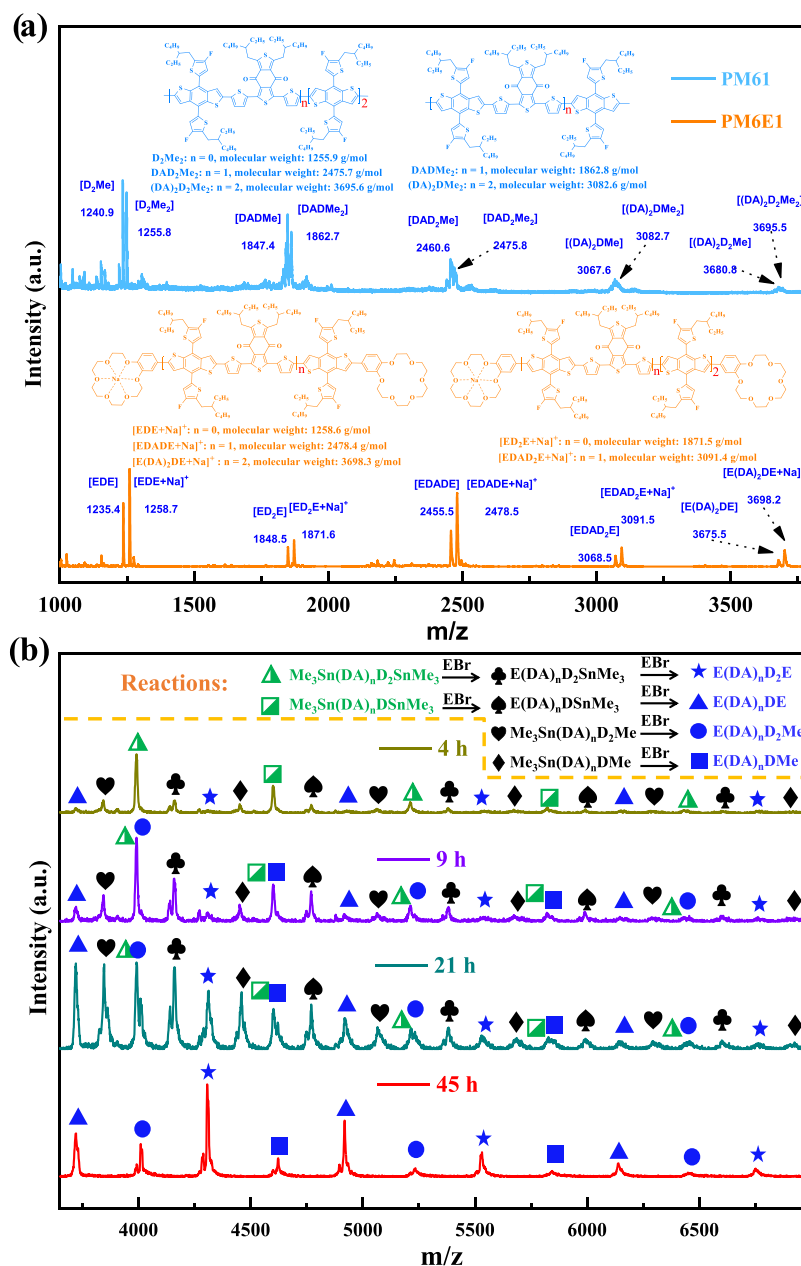


**Figure 1.** MALDI-TOF-MS spectra of (a) PM6E1 and PM61, and corresponding structures of some main peaks. (b) Polycondensation of PM6E4 for 4, 9, 21, and 45 h.

**Table 1.** Molecular Weights, End-Capping, and Optical Properties of the Polymers

polymer	ratio <sup>a</sup>	$M_t^b$ (kg/mol)	$M_n$ (kg/mol)	$M_w$ (kg/mol)	PDI	$C_{Tin}^c$ (%)	$Y_{MALDI}^d$ (%)	$Y_{NMR}^e$ (%)	$E_g^f$ (eV)
PM61	2:1	1.9							1.86
PM6E1	2:1	2.5					96	97	1.86
PM6E4	5:4	6.1	4.9	11.0	2.27	0.27	85	87	1.86
PM6E5	6:5	7.3	13.4	26.7	1.99	0.21	80	84	1.85
PM6E6	7:6	8.5	15.7	31.0	1.98	0.04	75	76	1.85
PM67	7:6	9.1	18.4	59.0	3.21	1.52			1.85
PM6E7	8:7	9.7	20.5	37.7	1.84	0.09	42	43	1.85
PM6E8	9:8	11.0	21.2	43.4	2.05	0.09	49	52	1.85
PM6E9	10:9	12.2	23.9	54.3	2.27	0.44	47	51	1.85

<sup>a</sup>Ratio of  $Me_3SnDSnMe_3/BrABr$ . <sup>b</sup>Estimated from the chemical structure. <sup>c</sup>Tin content in the polymer was determined by inductively coupled plasma mass spectrometry (ICP-MS). <sup>d</sup>Yield of end-capping by E was estimated from MALDI-TOF-MS. <sup>e</sup>Yield of end-capping by E was estimated from NMR. <sup>f</sup>Estimated from the onset of the absorption spectra of thin films.

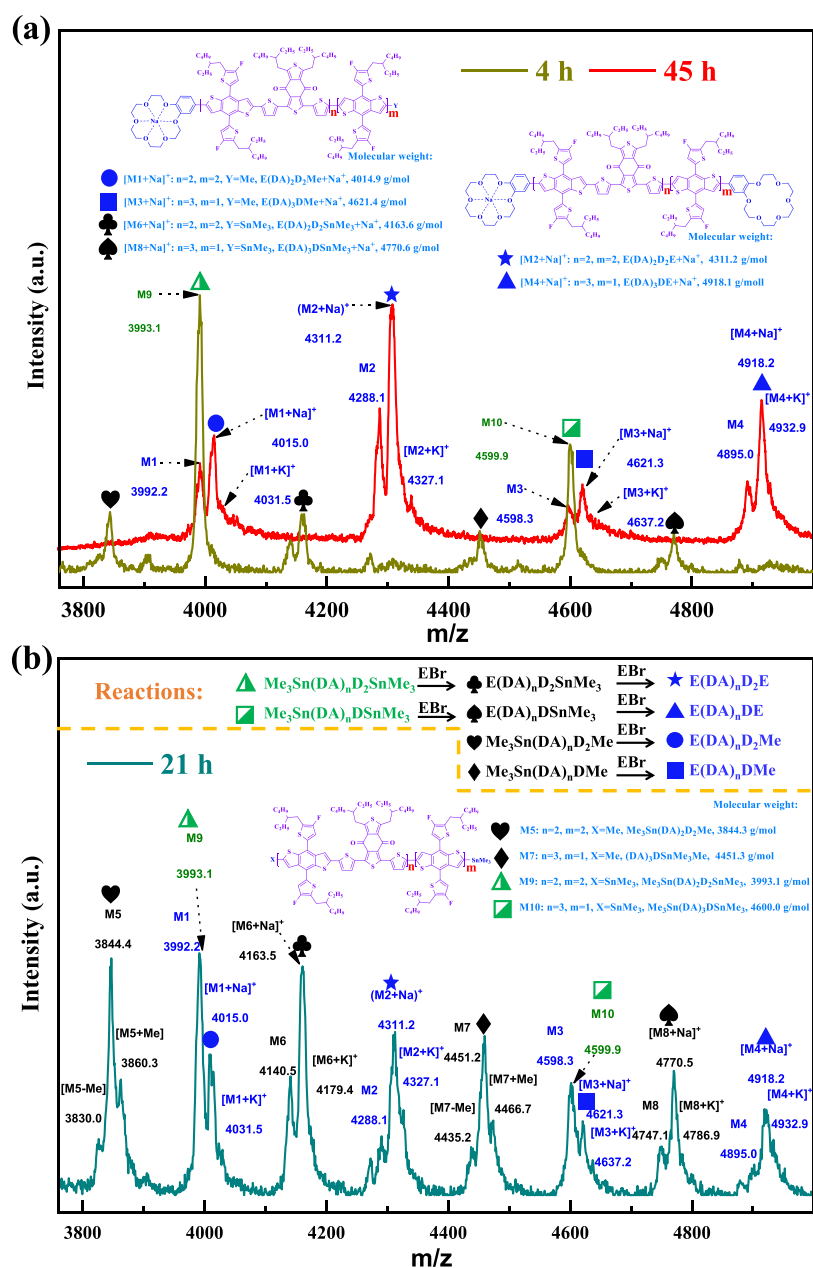


**Figure 2.** Enlarged MALDI-TOF-MS spectrum of the reaction to synthesized PM6E4 and corresponding chemical structures at (a) 45 h and (b) 21 h.

very clear peaks in both NMR (Figures S1 and S2 in the Supporting Information) and MALDI-TOF-MS (Figure 1a), indicating that PM6E1 exhibited a high yield of end-capping by E. Estimated from the peak areas in Figure 1a, the  $Y_{\text{MALDI}}$  was calculated to be 96%. The <sup>1</sup>H NMR spectrum of PM61 and PM6E1 in CDCl<sub>3</sub> is shown in Figures S1 and S2 in the Supporting Information, respectively. The  $Y_{\text{NMR}}$  was calculated to be 97% according to the ratio of H around 2.8 and 3.7 ppm in the spectrum. As both the  $Y_{\text{MALDI}}$  and  $Y_{\text{NMR}}$  were very high, this method was expected to synthesize polymers with high end-capping yields and other molecular weights. Then, MALDI-TOF-MS was also used to monitor the polymerization process to study the reaction conditions. For classification, PM6E4 was synthesized by fixing the D/A/E ratio to 5:4:2, with the results and corresponding structures shown in Figures 1b and 2. The spectra at 4, 21, and 45 h showed almost all of

the peaks and end-capping polymer peaks. Thus, they were sorted out and the corresponding chemical structures are depicted in Figure 2. It should be noted that peaks without end-capping were not found in the spectrum at 45 h. E(DA)<sub>n</sub>D<sub>2</sub>E, E(DA)<sub>n</sub>DE, E(DA)<sub>n</sub>D<sub>2</sub>Me, and E(DA)<sub>n</sub>DMe peaks were found in both curves at 21 and 45 h. These six more Me<sub>3</sub>Sn-containing molecules E(DA)<sub>n</sub>D<sub>2</sub>SnMe<sub>3</sub>, E(DA)<sub>n</sub>DSnMe<sub>3</sub>, Me<sub>3</sub>Sn(DA)<sub>n</sub>D<sub>2</sub>Me, Me<sub>3</sub>Sn(DA)<sub>n</sub>DMe, Me<sub>3</sub>Sn(DA)<sub>n</sub>D<sub>2</sub>SnMe<sub>3</sub>, and Me<sub>3</sub>Sn(DA)<sub>n</sub>DSnMe<sub>3</sub> in the spectrum at 21 h could react with EBr to give E(DA)<sub>n</sub>D<sub>2</sub>E, E(DA)<sub>n</sub>DE, E(DA)<sub>n</sub>D<sub>2</sub>Me, E(DA)<sub>n</sub>DMe, E(DA)<sub>n</sub>D<sub>2</sub>SnMe<sub>3</sub>, and E(DA)<sub>n</sub>DSnMe<sub>3</sub>, respectively.

As shown in Figure 1b, there were mainly Me<sub>3</sub>Sn-containing molecules in the mixture, while only a tiny amount of E(DA)<sub>n</sub>DE remained after reacting for 4 h at 90 °C. But no E(DA)<sub>n</sub>D<sub>2</sub>E, E(DA)<sub>n</sub>D<sub>2</sub>Me, and E(DA)<sub>n</sub>DMe peaks were

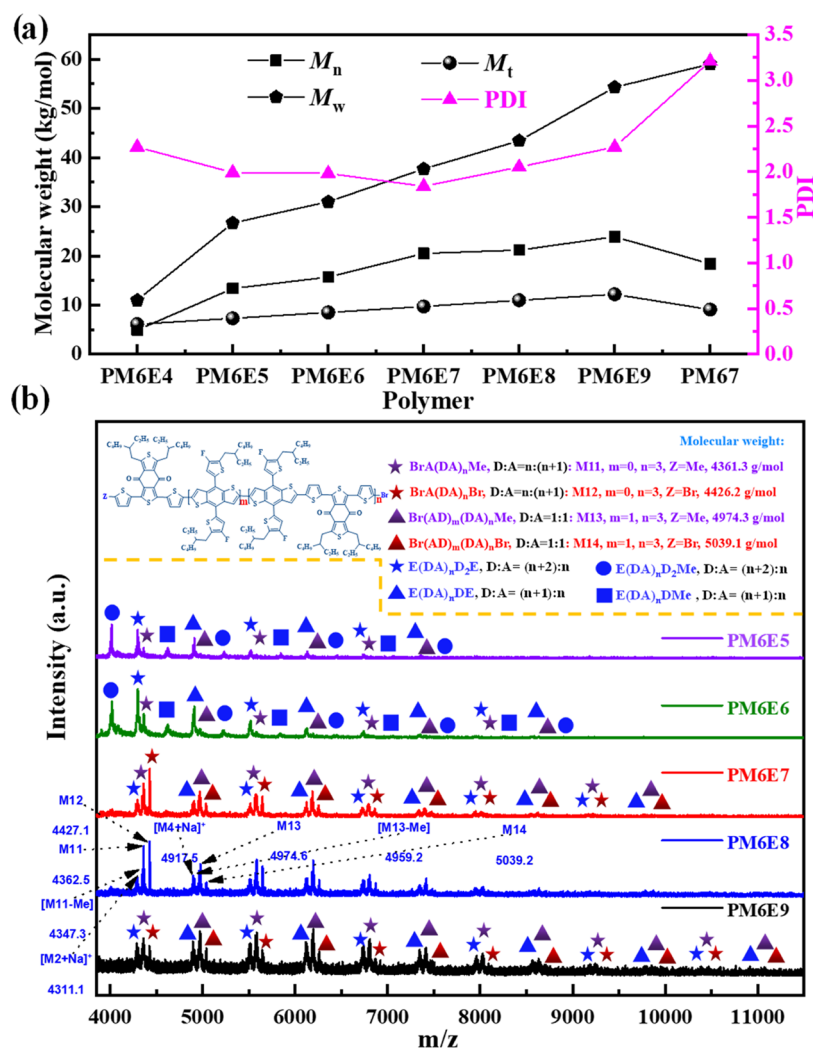


Figure 3. (a)  $M_n$ s,  $M_t$ s,  $M_w$ s, PDIs, and (b) MALDI-TOF-MS spectrum of PM6E*n* with some corresponding structures.

found, which means that the mixture preferred classical Stille coupling rather than side reactions (homocoupling and methylation), and there is a suitable energy gap between these reactions. This showed that a reaction with the catalyst  $\text{Pd}(\text{PPh}_3)_4$  at 90 °C could improve the chemoselectivity of polymerization rather than end-capping. When the mixture had reacted for 9 h, the distribution exhibited almost the same peak values with peak intensity increase. Besides, small amounts of  $\text{E}(\text{DA})_n\text{D}_2\text{E}$ ,  $\text{E}(\text{DA})_n\text{D}_2\text{Me}$ , and  $\text{E}(\text{DA})_n\text{DMe}$  peaks were also monitored. Then, after the high catalytic activity combination of  $\text{Pd}_2\text{dba}_3$  and  $\text{P}(o\text{-tol})_3$  was added, the mixture was heated at 90 and 110 °C for 6 and 30 h, respectively. When the mixture had reacted for 21 h, the corresponding MALDI-TOF-MS spectra showed more high  $m/z$  portions and most of the low-intensity peaks at 9 h increased quite a lot, especially some high  $m/z$  value peaks. This could be explained by the phenomenon that highly active  $\text{Pd}_2\text{dba}_3$  and  $\text{P}(o\text{-tol})_3$  at 110 °C could catalyze reactions much faster than  $\text{Pd}(\text{PPh}_3)_4$  at 90 °C, and the polycondensation, end-capping, and other reactions could all react effectively.<sup>23,36</sup> After the mixture had reacted for 45 h, many  $\text{Me}_3\text{Sn}$ -containing peaks were gone. In detail,  $\text{Me}_3\text{Sn}(\text{DA})_n\text{D}_2\text{SnMe}_3$  and  $\text{Me}_3\text{Sn}(\text{DA})_n\text{DSnMe}_3$  had reacted with 1 equiv of EBr to obtain  $\text{E}(\text{DA})_n\text{D}_2\text{SnMe}_3$  and  $\text{E}(\text{DA})_n\text{DSnMe}_3$ , respectively. The other four more  $\text{Me}_3\text{Sn}$  containing molecules  $\text{E}(\text{DA})_n\text{D}_2\text{SnMe}_3$ ,  $\text{E}(\text{DA})_n\text{DSnMe}_3$ ,

$\text{Me}_3\text{Sn}(\text{DA})_n\text{D}_2\text{Me}$ , and  $\text{Me}_3\text{Sn}(\text{DA})_n\text{DMe}$  also reacted with 1 equiv of EBr to give  $\text{E}(\text{DA})_n\text{D}_2\text{E}$ ,  $\text{E}(\text{DA})_n\text{DE}$ ,  $\text{E}(\text{DA})_n\text{D}_2\text{Me}$ , and  $\text{E}(\text{DA})_n\text{DMe}$ , respectively. These features indicated that the reaction intermediates were all converted, which meant the polycondensation and end-capping were finished. This also proved that  $\text{Pd}_2\text{dba}_3$  at 110 °C for 30 h could be long enough to make the mixture react completely. It should be noted that we did not further prolong the reaction time before or after adding  $\text{Pd}_2\text{dba}_3$  due to the consideration of the decomposition of the monomers and polymers. As shown in the spectrum at 45 h, all of the molecules were end-capped either by E or methyl with a yield of nearly 100%. The  $Y_{\text{MALDI}}$  and  $Y_{\text{NMR}}$  were estimated from the peak areas in the MALDI-TOF-MS spectrum at 45 h to be 85 and 87%, respectively (Figure S4 in the Supporting Information). The high end-capping yields indicating the protocol we proposed was very effective and was used to synthesize a series of polymers with different molecular weights.

The crude polymer was purified by Soxhlet extraction with methanol, acetone, hexane, and dichloromethane sequentially to remove the small molecular weight oligomers and other impurities.<sup>24</sup> PM6 (bought from Solarmer Materials Inc.), PM61, PM67, and PM6E*n* were characterized by NMR and chemical shift of peaks around 3.303 ppm could prove PM6E*n* was end-capped by EBr (Figures S1–S9 in the Supporting

Information). This could result in low Sn content and trap states, which should benefit photovoltaic performance improvement.<sup>23</sup> Then, these procedures were used as the standard protocol for the synthesis of all other polymers in this paper.

Following the protocol, a series of PM6En was synthesized by controlling the molar ratio of Me<sub>3</sub>SnDSnMe<sub>3</sub>/BrABr to be  $(m + 1)/m$ . When the ratio was over 10:9, the polymer started to be so insoluble in chloroform that could not be solution-processible to form a good film, which hindered its application. Gel permeation chromatography (GPC) was conducted to determine the number-average molecular weight ( $M_n$ ) with the corresponding weight-average molecular weight ( $M_w$ ) and PDI of each polymer. These parameters are summarized in Table 1 and plotted in Figure 3a,b.

As shown in Table 1, all of these polymers possessed relatively low PDIs below 2.27, except non-end-capped PM67, with a high PDI of 3.21. This is consistent with the MALDI-TOF-MS results (Figure 1a), indicating our protocol could synthesize polymers with narrow PDIs, which may also improve the performance of the target polymers. The theoretical molecular weight ( $M_t$ ),  $M_n$ , and  $M_w$  of PM6E4 were 6.1, 4.9, and 11.0 kg/mol, respectively. By decreasing the ratio to 6:5, the  $M_t$ ,  $M_n$ , and  $M_w$  of PM6E5 increased to 7.3, 13.4, and 26.7 kg/mol, respectively. As shown in Figure 3a, both the  $M_n$  and  $M_w$  of PM6En were substantially improved as the Me<sub>3</sub>SnDSnMe<sub>3</sub>/BrABr ratio increased, which is accorded with the concept of controlling polymer molecular weight by changing the monomer ratio in end-capped polycondensation. Changing the ratio to 10:9, PM6E9 was synthesized, and its  $M_t$ ,  $M_n$ , and  $M_w$  were 12.2, 23.9, and 54.3 kg/mol, respectively. There was a big difference among  $M_t$ ,  $M_n$ , and  $M_w$  as  $M_n$  and  $M_w$  were estimated from GPC measurements, which compared the particle size between the measured polymer with a polystyrene standard and calculated from different formulas. The GPC molecular weights were generally overestimated than the real molecular weight in this case due to conjugated PM6En being much more rigid and bulky than polystyrene when they have the same molecular weight.<sup>59,60</sup> The tin content ( $C_{\text{Tin}}$ ) in the polymer was determined by inductively coupled plasma mass spectrometry (ICP-MS), and the results were also summarized in Table 1. PM67 without end-capping had the highest tin content of 1.52%, while other polymers have low tin content below 0.5% due to end-capping. This suggested that the end-capping strategy could efficiently react with SnMe<sub>3</sub> and reduce the Tin content of the final polymer.

PM6En was also measured by MALDI-TOF-MS to estimate the yield of end-capping, and the spectrum is shown in Figure 3b. It should be noted that, as the D/A ratio increased, there were equal-D/A-ratio products  $\{[\text{Br}(\text{AD})_m(\text{DA})_n\text{Me}$  and  $\text{Br}(\text{AD})_m(\text{DA})_n\text{Br}]\}$  and high-A-ratio molecules  $\{[\text{BrA}(\text{DA})_n\text{Me}$  and  $\text{BrA}(\text{DA})_n\text{Br}]\}$ , besides the high-D-ratio polymers  $\{[\text{E}(\text{DA})_n\text{D}_2\text{E}$ ,  $\text{E}(\text{DA})_n\text{DE}$ ,  $\text{E}(\text{DA})_n\text{D}_2\text{Me}$ , and  $\text{E}(\text{DA})_n\text{DMe}]\}$ . As shown in Figures 1b and 2, when the ratio of D was high enough, only high-D-ratio molecules were observed, indicating that the homocoupling of two Me<sub>3</sub>SnDSnMe<sub>3</sub> became the main side reaction in the synthesis of both PM6E1 and PM6E4. When changed to PM6E5 and PM6E6, the monobromide equal-D/A and high-A-ratio molecules appeared and the end-capping yield dropped quite a lot. The dibromide equal-D/A and high-A-ratio molecules were found in PM6E7, PM6E8, and PM6E9. These results proved that the Stille polymerization was quite complicated,

while the homocoupling of SnMe<sub>3</sub>-containing compounds was very common in the synthesis of conjugated polymers, which resulted in nonregular products and bromide compounds.

All of these polymers exhibited reasonable end-capping yields (ranging from 40 to 97%), but the yield decreased as the D/A ratio decreased and side reactions possibility increased. Adding more end-capping reagents or using organotin-functionalized end-capping reagents would further increase the end-capping yield. The  $Y_{\text{NMR}}$  was higher than  $Y_{\text{MALDI}}$ , which may be due to the phenomenon that the crown ether group will hinder the packing between less polar aromatic rings and alkyl chains; hence, the end-capped molecules would be much more easy to be dispersed and soluble in deuterated chloroform than non-end-capped polymers. Thus, the saturated solution of polymers would enlarge the signal of end-capped portions as the NMR measurement was conducted at a relatively low temperature. The NMR peaks became much broader and more overlapped as the molecular weight increased, resulting in bad accuracy in estimating  $Y_{\text{NMR}}$  (Figures S1–S9 in the Supporting Information). Besides, the electron transfer matrix used in the MALDI-TOF-MS measurement was 2-[(2E)-3-(4-*tert*-butylphenyl)-2-methylprop-2-enylidene]malononitrile (DCTB). The ionization energy (IE) of DCTB and free 18-crown-6 were 8.5<sup>61</sup> and 9.7<sup>62</sup> eV, respectively. Thus, the MALDI-TOF-MS peaks of these polymers originated from the polymer backbone.  $Y_{\text{MALDI}}$  was underestimated since the end-capped polymers had higher molecular weights and showed weaker signals. Above all, this work proved that tuning the ratio of the monomers and end-capping reagent can control the molecular weight of PM6En effectively with a reasonable yield of end-capping at the same time.

**2.2. Optical and Electrochemical Properties.** The normalized UV–vis absorption spectra of polymers in a chloroform solution ( $1 \times 10^{-5}$  M) and in a thin film are shown in Figure S11a,b in the Supporting Information. As a typical D–A copolymer, PM6En exhibited two absorption bands—the low and high energy absorption bands can be attributed to the intramolecular charge transfer and the localized  $\pi$ – $\pi^*$  transition, respectively.<sup>38</sup> In going from a solution to a thin film, the absorption maximum bathochromically shifts about 5 nm. The absorption edge of PM6E1 is at 670 nm, corresponding to an optical band gap of 1.85 eV. The optical band gap slightly decreased to 1.84 eV as the conjugation length and molecular weight increased, indicating a higher light absorption ability and OSC short current density than PM6E4. The optical band gap is mainly determined by the intramolecular charge transfer from electron-rich benzo[1,2-*b*:4,5-*b'*]dithiophene (BDT) to electron-deficient 4*H*,8*H*-benzo[1,2-*c*:4,5-*c'*]dithiophene-4,8-dione (BDD). Although these polymers have different molecular weights and conjugate lengths, they all have the same sequence of benzo[1,2-*b*:4,5-*b'*]dithiophene (BDT) connected with 4*H*,8*H*-benzo[1,2-*c*:4,5-*c'*]dithiophene-4,8-dione (BDD). Thus, all of these polymers exhibit similar optical bandgaps, as shown in Table 1. PM6En exhibited similar light absorption properties, which were consistent with other reports.<sup>19,42</sup> To estimate the highest occupied molecular orbital (HOMO) and lowest unoccupied molecular orbital (LUMO) energy levels of these polymers, cyclic voltammetry (CV) measurement was performed, and the results are shown in Figure S11c,d in the Supporting Information. The HOMO energy levels of PM6E5, PM67, PM6E7, and PM6E9 were estimated to be  $-5.70$ ,  $-5.77$ ,

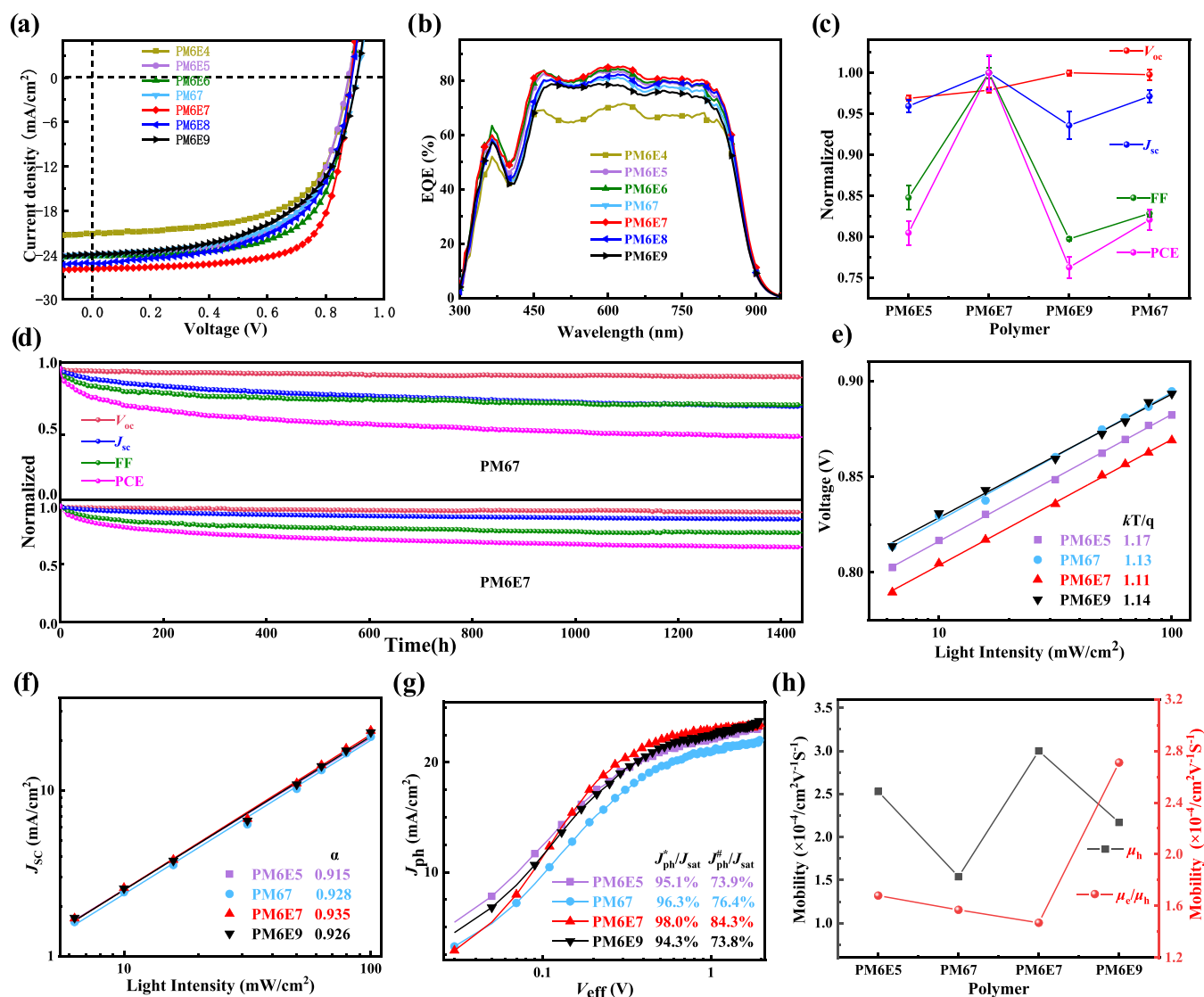


**Figure 4.** (a) Current–voltage, (b) EQE, (c) normalized  $V_{oc}$ ,  $J_{sc}$ , fill factor (FF), PCE characteristic of polymer:L8-BO solar cells under AM 1.5 conditions ( $100 \text{ mW/cm}^2$ ). (d) Light-soak stability of the polymer:L8-BO device under continuous illumination ( $100 \text{ mW/cm}^2$ ). (e)  $V_{oc}$  and (f)  $J_{sc}$  of the OSC dependence on  $P_{\text{light}}$ . (g)  $J_{\text{ph}}-V_{\text{eff}}$  curves and (h)  $\mu_h$  and  $\mu_e/\mu_h$  of devices.

**Table 2. Photovoltaic Properties of OSCs Based on PM6En and PM67**

polymer	$V_{oc}$ (V)	$J_{sc}$ ( $\text{mA/cm}^2$ )	FF (%)	PCE <sup>a</sup> (%)
PM6E4	0.877 (0.879 ± 0.003)	21.27 (20.91 ± 0.62)	62.71 (62.49 ± 1.18)	11.70 (11.48 ± 0.22)
PM6E5	0.876 (0.872 ± 0.003)	24.05 (24.11 ± 0.20)	61.15 (60.11 ± 1.01)	12.89 (12.63 ± 0.23)
PM6E6	0.886 (0.880 ± 0.004)	24.76 (24.59 ± 0.16)	66.07 (65.33 ± 0.54)	14.50 (14.14 ± 0.25)
PM67	0.905 (0.898 ± 0.006)	24.58 (24.41 ± 0.18)	58.88 (58.74 ± 0.31)	13.10 (12.88 ± 0.19)
PM6E7	0.885 (0.881 ± 0.003)	25.87 (25.13 ± 0.50)	71.02 (70.89 ± 0.47)	16.26 (15.69 ± 0.34)
PM6E8	0.888 (0.884 ± 0.003)	25.09 (24.71 ± 0.31)	59.68 (59.90 ± 0.66)	13.29 (13.08 ± 0.22)
PM6E9	0.904 (0.900 ± 0.003)	23.88 (23.52 ± 0.42)	56.48 (56.54 ± 0.18)	12.20 (11.97 ± 0.21)

<sup>a</sup>In parentheses are average values based on more than eight devices.

–5.67, and –5.68, respectively. Compared to PM67, the end-capped polymers exhibited higher energy levels, which may be due to the electron-donating ability of benzo-18-crown-6.

**2.3. Photovoltaic Properties.** Conventional OSCs were fabricated with the following device structure: indium tin oxide (ITO)/PEDOT:PSS/polymer:L8-BO/PFN-Br/Al, where PEDOT:PSS and PFN-Br are poly(3,4-ethylenedioxythiophene)/polystyrenesulfonate and poly[(9,9-bis(3'-(*N,N*-dimethyl)-*N*-ethylammonium)-propyl)-2,7-fluorene-*alt*-2,7-(9,9-

diocetylfluorene)]dibromide, respectively. The current density–voltage ( $J-V$ ) characteristics of these devices were measured under the simulated solar illumination of  $100 \text{ mW/cm}^2$ . The  $J-V$  and external quantum efficiency (EQE) curves are shown in Figure 4a,b, and the device parameters are summarized in Table 2. The highly polar benzo-18-crown-6 has some bad effects on the photovoltaic performance of PM6En.

The PM6E4-based best device exhibited a high  $V_{oc}$  of 0.877 but a small  $J_{sc}$  of  $21.27 \text{ mA/cm}^2$  and a low FF of 62.71%, all of

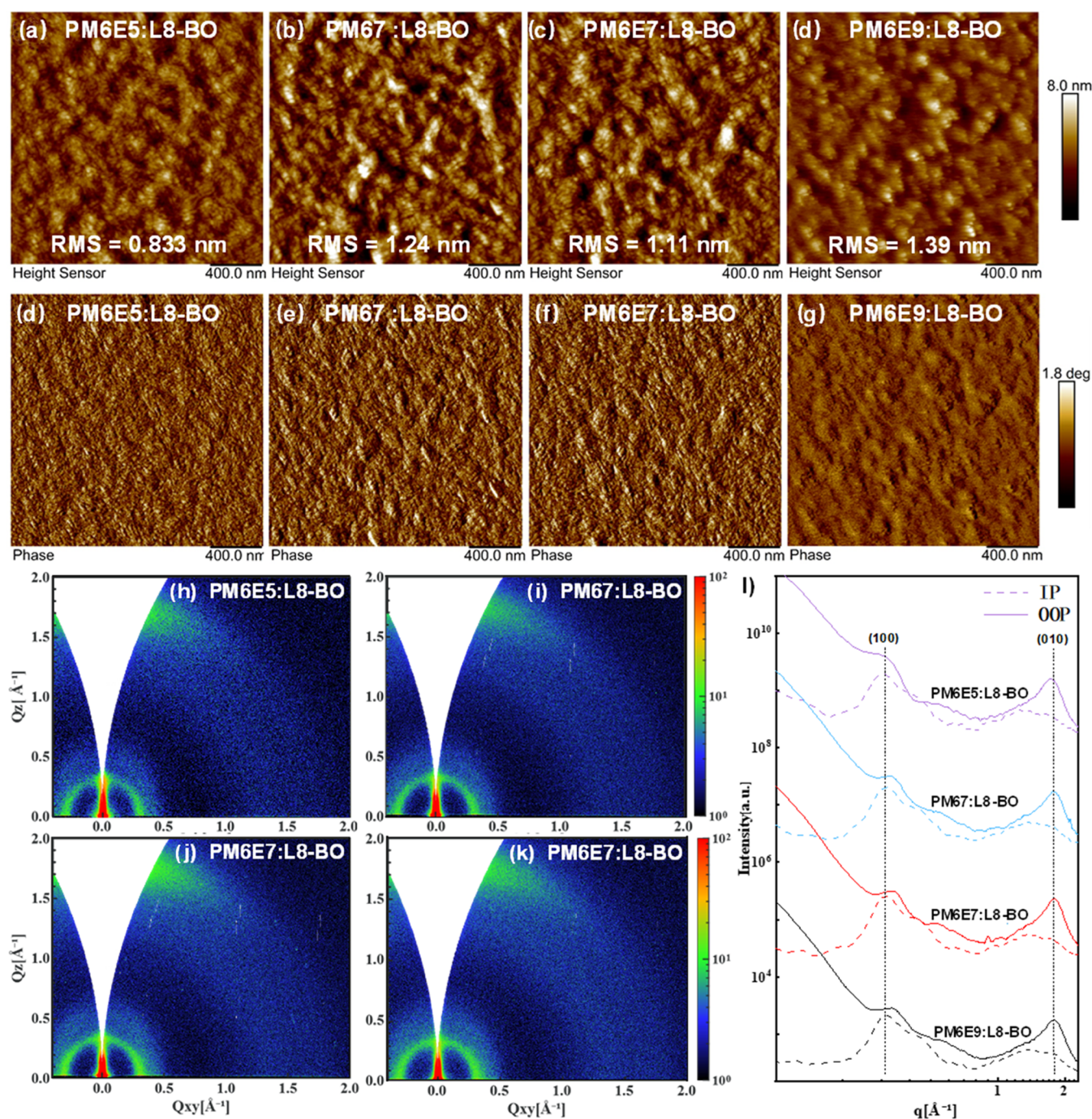


**Figure 5.** AFM height images of (a) PM6E5:L8-BO, (b) PM67:L8-BO, (c) PM6E7:L8-BO, and (d) PM6E9:L8-BO blends. AFM phase images of (d) PM6E5:L8-BO, (e) PM67:L8-BO, (f) PM6E7:L8-BO, and (g) PM6E9:L8-BO blends. 2D GIWAXS patterns of (h) PM6E5:L8-BO, (i) PM67:L8-BO, (j) PM6E7:L8-BO, and (k) PM6E9:L8-BO blends. (l) Scattering profiles of out-of-plane and in-plane directions for the optimized blend films.

which contribute to a poor PCE of 11.70%. In going from PM6E4 to PM6E5, PM6E6, and PM6E7, with the increase in molecular weight, the corresponding OSCs showed an even higher efficiency. The PM6E7-based device showed a remarkable PCE of 16.26%, with the highest  $J_{SC}$  of 25.87  $\text{mA}/\text{cm}^2$ , an FF of 71.02%, and a reasonable  $V_{oc}$  of 0.885 V. When changed to PM67, the corresponding best OSC exhibited a lower PCE of 13.10% with a poor FF of 58.88%. But a further increase of molecular weight led to bad photovoltaic performance, which was consistent with other reports.<sup>43</sup>

For simplicity and clarity, four polymers were selected to study the variation of photovoltaic performance. As shown in Figure 4c, as the molecular weight increased (from PM6E5 to PM6E7 and PM6E9), the  $V_{oc}$  was continuously enhanced. But  $J_{sc}$ , FF, and PCE first improved and then decreased. Compared to PM6E7, non-end-capped PM67 exhibited poorer  $J_{sc}$ , FF, and PCE, which may be due to high tin contents and poor micromorphology. The PM6E7-based OSCs showed the best PCE,  $J_{sc}$ , and FF among these polymers, indicating that both the molecular weights and end-capping have significant effects on the photovoltaic performance of OSCs. The light-soak

stability of the polymer:L8-BO device under continuous illumination ( $100 \text{ mW/cm}^2$ ) was also conducted and the results are plotted in Figure 4d. Compared to PM67, the end-capped PM6E7-based OSCs exhibited better  $V_{oc}$ ,  $J_{sc}$ , FF, and PCE stability. Especially the obvious  $J_{sc}$  enhancement may be due to low traps caused by tin content and stable morphology. After 1400 h of continuous illumination, the normalized PCE of PM6E7- and PM67-based OSCs dropped to 64.7 and 48.7%, respectively. The 33% PCE stability enhancement indicated that the end-capping can effectively improve stability.

To reveal the origin of the performance of the OSCs, the effects of  $V_{oc}$  and  $J_{sc}$  on light intensity ( $P_{light}$ ) were measured, and the corresponding characteristics are plotted in Figure 4e,f. The dependence of  $J_{sc}$  and  $V_{oc}$  on  $P_{light}$  can be described as  $J_{sc} \propto P_{light}^\alpha$  and  $V_{oc} \propto nkT/q \ln P_{light}$ , respectively. Thereinto, the bimolecular recombination can be completely suppressed when the  $\alpha$  value is equal to 1, and the trap-assisted recombination can be negligible if the  $n$  value is close to 1.<sup>63,64</sup> The  $\alpha$  and  $n$  values are 0.915/1.17, 0.928/1.13, 0.935/1.11, and 0.926/1.14 for the PM6E5-, PM67-, PM6E7-, and PM6E9-based OSCs, respectively. The  $\alpha$  value of the PM6E7-based device was the closest to 1 among these polymer-based OSCs, suggesting negligible bimolecular recombination and more significant charge carrier transportation. The  $n$  is also very close to 1, indicating that trap-assisted recombination and geminate recombination were effectively suppressed. The enhancement of  $\alpha$  and  $n$  can well explain their photovoltaic performance. As a result, the PM6E7-based OSCs exhibited the most efficient exciton dissociation and minimal charge carrier recombination possibility, boosting their FF and PCE to 71.02 and 16.26%, respectively.

To further investigate the origin of the charge dissociation and collection properties in the blend films, the dependency of the photocurrent density ( $J_{ph} = J_L - J_D$ , where  $J_L$  and  $J_D$  are the current densities of the devices under illumination and in the dark, respectively) versus the effective voltage ( $V_{eff} = V_0 - V_{bias}$ , where  $V_0$  is the voltage when  $J_{ph}$  is zero and  $V_{bias}$  is the applied voltage bias) of the devices were measured (shown in Figure 4g). Both the  $J_{ph}^*/J_{sat}$  and  $J_{ph}^\# / J_{sat}$  are calculated to measure exciton dissociation and charge collection efficiencies, respectively. The  $J_{ph}^*$ ,  $J_{ph}^\#$ , and  $J_{sat}$  represent the  $J_{ph}$  under short-circuit, maximum power output, and ideal (all of the photogenerated excitons are dissociated into free charge carriers and then collected by electrodes) conditions, respectively.<sup>65,66</sup> The relatively large  $J_{sat}$  of PM6E7-based OSCs should be attributed to the suitable molecular weight and morphology. The exciton dissociation and charge collection efficiencies are estimated to be 95.1/73.9, 96.3/76.3, 98.0/84.3, and 94.3/73.8% for the PM6E5-, PM67-, PM6E7-, and PM6E9-based OSCs, respectively. The  $J_{sc}$ s and FFs of devices were increased as the exciton dissociation and charge collection efficiencies enhanced.

Moreover, the space charge limit current (SCLC) method was used to measure the hole and electron mobilities ( $\mu_h$  and  $\mu_e$ ) of the binary blends (Figures 4h and S12 in the Supporting Information). All end-capped polymers showed better hole mobilities than non-end-capped PM67, which may be due to fewer end traps. The hole mobility was also raised as molecular weight increased, which is consistent with other reports.<sup>43</sup> The polymers also had significant effects on the electron mobilities of the blend films. As a result, the  $\mu_e/\mu_h$  has been continuously decreased to 1.47 as the molecular weight of the polymer

increased until a huge increase at PM6E9. This could explain the photovoltaic performance changes, especially the FF.

**2.4. Nanomorphology of the Blend Films.** The morphology of the active layer was closely related to the charge carrier transfer/transport processes and photovoltaic performance. Hence, atomic force microscopy (AFM) was performed, and the images are shown in Figure 4a–g. The PM67:L8-BO and PM6E7:L8-BO films had clearer phase separation and moderate root-mean-square (RMS) roughness than PM6E5:L8-BO and PM6E9:L8-BO films, which may be the reason for the difference in their photovoltaic performance. The “fibril” diameters of PM6E5:L8-BO, PM67:L8-BO, PM6E7:L8-BO, and PM6E9:L8-BO were 22, 26, 32, and 20 nm, respectively. As the “fibril” size increased, the charge generation/transport to electrodes became much more efficient, resulting in better  $J_{sc}$ , FF, and PCE.

High crystallinity is beneficial for suppressed charge recombination, improved carrier transport characteristics, and photovoltaic performance. Thus, the grazing-incidence wide-angle X-ray scattering (GIWAXS) measurements were conducted to investigate the effects of different formulas on molecular stacking and crystallinity. As shown in the two-dimensional (2D) GWAXS patterns (Figure 5g–k), as well as the corresponding out-of-plane and in-plane line cut profiles (Figure S1), the blend films based on polymer:L8-BO exhibited pronounced scattering peaks (010) in the out-of-plane (OOP) direction and highly ordered lamellar stacking peaks (100) in the in-plane direction, indicating that these films had similar crystallinity.

All of these films showed the  $\pi$ – $\pi$  stacking and diffraction peaks at  $\approx 1.79 \text{ \AA}^{-1}$  from the line cuts of the OOP direction and  $0.309 \text{ \AA}^{-1}$  in the IP orientation. According to the Scherrer equation, the crystalline coherence lengths (CCLs) of the blend films based on PM6E5, PM67, PM6E7, and PM6E9 were calculated to be 66.86, 67.34, 76.64, and 64.49  $\text{\AA}$ , respectively. The PM6E7:L8-BO films possessed the highest CCL value, reflecting that it was more crystallized than others. The change of CCLs reflected the crystallinity of the films, which was consistent with the PCEs. These results indicated that tuning the monomer ratio of monomers and end-capping reagents can effectively control the crystallinity and photovoltaic performance of polymers. The CCLs of PM6E5-, PM67-, PM6E7-, and PM6E9-based blend films in the OOP direction were estimated to be 16.33, 16.88, 17.68, and 16.01  $\text{\AA}$ , respectively. It showed that both the molecular weight and end-capping affected the crystallinity of the active layer. PM6E7 exhibited the highest crystallinity value than the non-end-capping polymer or other polymers with different molecular weights. The crystallinity tendency was perfectly accordant with the device performance (FF and PCE, especially), which was mainly responsible for the ordered packing in the PM6E7:L8-BO film.

### 3. CONCLUSIONS

In summary, a novel molecular weight-controllable end-capped copolymer synthesis strategy was realized by changing the ratio of the end-capping reagent, donor, and acceptor monomers. MALDI-TOF-MS was conducted to monitor the polycondensation process and decide when the reaction was complete. These procedures were used as the standard protocol for end-capping polymer synthesis. By changing the molar ratio between monomers, a series of PM6E*n* was synthesized efficiently. It is so difficult to measure the low content of end

groups precisely because there is no end-capping yield report in OSCs. 4'-bromobenzo-18-crown-6 was chosen as the end-capping reagent because it could be clearly distinguished from PM6. The end-capping efficiency of PM6En was over 40%, which was estimated by both MALDI-TOF-MS and NMR for the first time. GPC was conducted to estimate the  $M_n$ ,  $M_w$ , and PDI. As the ratio of  $\text{Me}_3\text{SnDSnMe}_3$  and BrABr decreased, both the  $M_n$  and  $M_w$  exhibited an approximate linear growth. PM6En showed narrow PDIs and similar light absorption features, but the optical band gap decreased slightly as the molecular weight increased. The performance of OSCs based on PM6En:L8-BO depended on their molecular weight, which can be finely tuned by controlling the ratio of  $\text{Me}_3\text{SnDSnMe}_3$ :BrABr. OSCs based on PM6E4:L8-BO showed an inferior efficiency of 11.70% with a high  $V_{oc}$  of 0.877 V due to the low molecular weight of PM6E4. The best OSCs with PM6E7 achieved the highest PCE of 16.26% and better stability than the non-end-capped PM67. The performance enhancement was owing to suitable molecular weight, better micromorphology, fewer end traps, higher crystallinity, and balanced mobility. Generally, higher-molecular-weight polymers may have better molecular packing, crystallinity, and charge transport but decrease the solubility and interrupt the packing of acceptors. PM6E7 happens to balance the interaction with L8-BO, resulting in suitable crystallinity, molecular packing, and charge transport and the best photovoltaic performance.<sup>2,12–16</sup> How to further improve the end-capping yield is still challenging and important to regulate the polymer performance. Furthermore, we are working on synthesizing functional end-capped polymers to regulate their photovoltaic performance. These findings and detailed studies paved important guidance to tune and optimize copolymers' molecular weights and properties for high-performance OSCs and other applications.

## ■ ASSOCIATED CONTENT

### SI Supporting Information

The Supporting Information is available free of charge at <https://pubs.acs.org/doi/10.1021/acs.macromol.3c00798>.

Materials, instruments, synthesis, fabrication, and characterization of OSCs,  $^1\text{H}$  NMR spectrum of polymers, GPC measurements, UV–vis absorption measurements, mobility measurements, thermogravimetric analysis (TGA) curves, cyclic voltammograms, other characterizations, and photovoltaic performance of OSCs based on the polymer:L8-BO blend films (PDF)

## ■ AUTHOR INFORMATION

### Corresponding Authors

**Lijun Li** – College of Chemistry and Environmental Science, Key Laboratory of Chemical Biology of Hebei Province, Key Laboratory of Medicinal Chemistry and Molecular Diagnosis, Ministry of Education, Hebei University, Baoding 071002, P. R. China; Email: [lj@hbu.edu.cn](mailto:lj@hbu.edu.cn)

**Jinchong Xiao** – College of Chemistry and Environmental Science, Key Laboratory of Chemical Biology of Hebei Province, Key Laboratory of Medicinal Chemistry and Molecular Diagnosis, Ministry of Education, Hebei University, Baoding 071002, P. R. China; [orcid.org/0000-0002-5451-220X](https://orcid.org/0000-0002-5451-220X); Email: [jxiaoc@163.com](mailto:jxiaoc@163.com)

**Meng Wang** – i-Lab & Printable Electronics Research Center, Suzhou Institute of Nano-Tech and Nano-Bionics, Chinese

Academy of Sciences, Suzhou 215123, P. R. China; School of Nano-Tech and Nano-Bionics, University of Science and Technology of China, Hefei 230027, P. R. China;

[orcid.org/0000-0003-3607-4071](https://orcid.org/0000-0003-3607-4071); Email: [mwang2021@sinano.ac.cn](mailto:mwang2021@sinano.ac.cn)

**Chang-Qi Ma** – i-Lab & Printable Electronics Research Center, Suzhou Institute of Nano-Tech and Nano-Bionics, Chinese Academy of Sciences, Suzhou 215123, P. R. China; School of Nano-Tech and Nano-Bionics, University of Science and Technology of China, Hefei 230027, P. R. China; [orcid.org/0000-0002-9293-5027](https://orcid.org/0000-0002-9293-5027); Email: [cqma2011@sinano.ac.cn](mailto:cqma2011@sinano.ac.cn)

### Authors

**Yiming Li** – College of Chemistry and Environmental Science, Key Laboratory of Chemical Biology of Hebei Province, Key Laboratory of Medicinal Chemistry and Molecular Diagnosis, Ministry of Education, Hebei University, Baoding 071002, P. R. China; i-Lab & Printable Electronics Research Center, Suzhou Institute of Nano-Tech and Nano-Bionics, Chinese Academy of Sciences, Suzhou 215123, P. R. China

**Jiaqing Liu** – College of Mechanics and Materials, Hohai University, Nanjing 210098, P. R. China

**Ke Shui** – Henan Institute of Advanced Technology, Zhengzhou University, Zhengzhou 450052, P. R. China

**Fan Xie** – Henan Institute of Advanced Technology, Zhengzhou University, Zhengzhou 450052, P. R. China

**Xuan Li** – College of Chemistry and Environmental Science, Key Laboratory of Chemical Biology of Hebei Province, Key Laboratory of Medicinal Chemistry and Molecular Diagnosis, Ministry of Education, Hebei University, Baoding 071002, P. R. China; i-Lab & Printable Electronics Research Center, Suzhou Institute of Nano-Tech and Nano-Bionics, Chinese Academy of Sciences, Suzhou 215123, P. R. China

**Yi Lin** – Department of Chemistry, Xi'an Jiaotong Liverpool University, Suzhou 215123, P. R. China; [orcid.org/0000-0001-9478-152X](https://orcid.org/0000-0001-9478-152X)

**Zehua Zhou** – College of Mechanics and Materials, Hohai University, Nanjing 210098, P. R. China

**Qing Zhang** – Vacuum Interconnected Nanotech Workstation (Nano-X), Suzhou Institute of Nano-Tech and Nano-Bionics of Chinese Academy of Sciences, Suzhou 215123, P. R. China

**Fengqi Guo** – Henan Institute of Advanced Technology, Zhengzhou University, Zhengzhou 450052, P. R. China

Complete contact information is available at:

<https://pubs.acs.org/doi/10.1021/acs.macromol.3c00798>

### Author Contributions

The manuscript was written through contributions of all authors. All authors have given approval to the final version of the manuscript.

### Notes

The authors declare no competing financial interest.

## ■ ACKNOWLEDGMENTS

This study is jointly supported by the NSFC (52203249), the Young Innovation Leading Talents of Suzhou Innovation and Entrepreneurship Leading Talents Program (ZXL2022462), the Young Elite Scientists Sponsorship Program by the Suzhou Association for Science and Technology (E2391303), and the Suzhou Institute of Nano-Tech and Nano-Bionics, Chinese Academy of Sciences (E1511401). The authors would also like

to thank the technical support for Nano-X from the Suzhou Institute of Nano-Tech and Nano-Bionics, Chinese Academy of Science (No. A2107).

## REFERENCES

- (1) Liang, Y.; Zhang, D.; Wu, Z.; Jia, T.; Lüer, L.; Tang, H.; Hong, L.; Zhang, J.; Zhang, K.; Brabec, C. J.; Li, N.; Huang, F. Organic solar cells using oligomer acceptors for improved stability and efficiency. *Nat. Energy* **2022**, *7*, 1180–1190.
- (2) Wang, J.; Xue, P.; Jiang, Y.; Huo, Y.; Zhan, X. The principles, design and applications of fused-ring electron acceptors. *Nat. Rev. Chem.* **2022**, *6*, 614–634.
- (3) Zhan, L.; Li, S.; Li, Y.; Sun, R.; Min, J.; Chen, Y.; Fang, J.; Ma, C.-Q.; Zhou, G.; Zhu, H.; Zuo, L.; Qiu, H.; Yin, S.; Chen, H. Manipulating Charge Transfer and Transport via Intermediary Electron Acceptor Channels Enables 19.3% Efficiency Organic Photovoltaics. *Adv. Energy Mater.* **2022**, *12*, No. 2201076.
- (4) Gao, J.; Yu, N.; Chen, Z.; Wei, Y.; Li, C.; Liu, T.; Gu, X.; Zhang, J.; Wei, Z.; Tang, Z.; Hao, X.; Zhang, F.; Zhang, X.; Huang, H. Over 19.2% Efficiency of Organic Solar Cells Enabled by Precisely Tuning the Charge Transfer State Via Donor Alloy Strategy. *Adv. Sci.* **2022**, *9*, No. 2203606.
- (5) Chong, K.; Xu, X.; Meng, H.; Xue, J.; Yu, L.; Ma, W.; Peng, Q. Realizing 19.05% Efficiency Polymer Solar Cells by Progressively Improving Charge Extraction and Suppressing Charge Recombination. *Adv. Mater.* **2022**, *34*, No. 2109516.
- (6) Cui, Y.; Xu, Y.; Yao, H.; Bi, P.; Hong, L.; Zhang, J.; Zu, Y.; Zhang, T.; Qin, J.; Ren, J.; Chen, Z.; He, C.; Hao, X.; Wei, Z.; Hou, J. Single-Junction Organic Photovoltaic Cell with 19% Efficiency. *Adv. Mater.* **2021**, *33*, No. 2102420.
- (7) Wei, Y.; Chen, Z.; Lu, G.; Yu, N.; Li, C.; Gao, J.; Gu, X.; Hao, X.; Lu, G.; Tang, Z.; Zhang, J.; Wei, Z.; Zhang, X.; Huang, H. Binary Organic Solar Cells Breaking 19% via Manipulating Vertical Component Distribution. *Adv. Mater.* **2022**, *34*, No. 2204718.
- (8) He, C.; Pan, Y.; Ouyang, Y.; Shen, Q.; Gao, Y.; Yan, K.; Fang, J.; Chen, Y.; Ma, C.-Q.; Min, J.; Zhang, C.; Zuo, L.; Chen, H. Manipulating the D:A interfacial energetics and intermolecular packing for 19.2% efficiency organic photovoltaics. *Energy Environ. Sci.* **2022**, *15*, 2537–2544.
- (9) Zheng, Z.; Wang, J.; Bi, P.; Ren, J.; Wang, Y.; Yang, Y.; Liu, X.; Zhang, S.; Hou, J. Tandem Organic Solar Cell with 20.2% Efficiency. *Joule* **2022**, *6*, 171–184.
- (10) Zhang, D.; Fan, B.; Ying, L.; Li, N.; Brabec, C. J.; Huang, F.; Cao, Y. Recent progress in thick-film organic photovoltaic devices: Materials, devices, and processing. *SusMat* **2021**, *1*, 4–23.
- (11) Zhang, G.; Zhao, J.; Chow, P. C. Y.; Jiang, K.; Zhang, J.; Zhu, Z.; Zhang, J.; Huang, F.; Yan, H. Nonfullerene Acceptor Molecules for Bulk Heterojunction Organic Solar Cells. *Chem. Rev.* **2018**, *118*, 3447–3507.
- (12) Meng, D.; Zheng, R.; Zhao, Y.; Zhang, E.; Dou, L.; Yang, Y. Near-infrared Materials: The Turning Point of Organic Photovoltaics. *Adv. Mater.* **2022**, *34*, No. 2107330.
- (13) Liu, Z.-X.; Yu, Z.-P.; Shen, Z.; He, C.; Lau, T.-K.; Chen, Z.; Zhu, H.; Lu, X.; Xie, Z.; Chen, H.; Li, C.-Z. Molecular insights of exceptionally photostable electron acceptors for organic photovoltaics. *Nat. Commun.* **2021**, *12*, No. 3049.
- (14) Xiang, W.; Xu, X.; Huang, Y.; Yu, L.; Li, R.; Jiang, Y.; Peng, Q. Verifying the structure-property-performance relationship of Y6-based small molecule acceptors by alkoxy-side chain isomerization and conjugated skeleton asymmetry. *Chem. Eng. J.* **2022**, *441*, No. 136058.
- (15) Ren, J.; Bi, P.; Zhang, J.; Liu, J.; Wang, J.; Xu, Y.; Wei, Z.; Zhang, S.; Hou, J. Molecular design revitalizes the low-cost PTV-polymer for highly efficient organic solar cells. *Natl. Sci. Rev.* **2021**, *8*, No. nwab031.
- (16) Lee, J.; Kim, J. W.; Park, S. A.; Son, S. Y.; Choi, K.; Lee, W.; Kim, M.; Kim, J. Y.; Park, T. Study of Burn-In Loss in Green Solvent-Processed Ternary Blended Organic Photovoltaics Derived from UV-Crosslinkable Semiconducting Polymers and Nonfullerene Acceptors. *Adv. Energy Mater.* **2019**, *9*, No. 1901829.
- (17) Yuan, X.; Zhao, Y.; Zhan, T.; Oh, J.; Zhou, J.; Li, J.; Wang, X.; Wang, Z.; Pang, S.; Cai, P.; Yang, C.; He, Z.; Xie, Z.; Duan, C.; Huang, F.; Cao, Y. A Donor Polymer Based on 3-Cyanothiophene with Superior Batch-to-Batch Reproducibility for High-Efficiency Organic Solar Cells. *Energy Environ. Sci.* **2021**, *14*, 5530–5540.
- (18) Ma, B.; Shi, Q.; Ma, X.; Li, Y.; Chen, H.; Wen, K.; Zhao, R.; Zhang, F.; Lin, Y.; Wang, Z.; Huang, H. Defect-Free Alternating Conjugated Polymers Enabled by Room-Temperature Stille Polymerization. *Angew. Chem., Int. Ed.* **2022**, *61*, No. e202115969.
- (19) Lee, B.; Kim, S.; Nho, H.-W.; Oh, J.; Park, G.; Jeong, M.; Cho, Y.; Lee, S. M.; Kwon, O.-H.; Yang, C. Viable Mixing Protocol Based on Formulated Equations for Achieving Desired Molecular Weight and Maximal Charge Separation of Photovoltaic Polymer. *Adv. Energy Mater.* **2021**, *11*, No. 2102594.
- (20) Fan, Q.; Fu, H.; Wu, Q.; Wu, Z.; Lin, F.; Zhu, Z.; Min, J.; Wu, H. Y.; Jen, A. K.-Y. Multi-Selenophene-Containing Narrow Bandgap Polymer Acceptors for All-Polymer Solar Cells with over 15% Efficiency and High Reproducibility. *Angew. Chem., Int. Ed.* **2021**, *60*, 15935–15943.
- (21) Jia, J.; Huang, Q.; Jia, T.; Zhang, K.; Zhang, J.; Miao, J.; Huang, F.; Yang, C. Fine-Tuning Batch Factors of Polymer Acceptors Enables a Binary All-Polymer Solar Cell with High Efficiency of 16.11%. *Adv. Energy Mater.* **2022**, *12*, No. 2103193.
- (22) Kong, J.; Song, S.; Yoo, M.; Lee, G. Y.; Kwon, O.; Park, J. K.; Back, H.; Kim, G.; Lee, S. H.; Suh, H.; Lee, K. Long-term stable polymer solar cells with significantly reduced burn-in loss. *Nat. Commun.* **2014**, *5*, No. 5688.
- (23) Zheng, B.; Yue, Y.; Ni, J.; Sun, R.; Min, J.; Wang, J.; Jiang, L.; Huo, L. An end-capped strategy for crystalline polymer donor to improve the photovoltaic performance of non-fullerene solar cells. *Sci. China: Chem.* **2022**, *65*, 964–972.
- (24) Li, Y.; Wang, M.; Zhang, Q.; Wu, Z.; Lim, H.; Wang, Y.; Qin, H.; Yang, J.; Gao, C.; Young Woo, H.; Yuan, J. Fine-tuned crystallinity of polymerized non-fullerene acceptor via molecular engineering towards efficient all-polymer solar cell. *Chem. Eng. J.* **2022**, *428*, No. 131232.
- (25) Parr, Z. S.; Borges-Gonzalez, J.; Rashid, R. B.; Thorley, K. J.; Meli, D.; Paulsen, B. D.; Strzalka, J.; Rivnay, J.; Nielsen, C. B.; Borges-Gonzalez, J. From p- to n-Type Mixed Conduction in Isoindigo-Based Polymers through Molecular Design. *Adv. Mater.* **2022**, *34*, No. 2107829.
- (26) Su, W.; Fan, Q.; Jalan, I.; Wang, Y.; Peng, W.; Guo, T.; Zhu, W.; Yu, D.; Hou, L.; Moons, E.; Wang, E. Nonconjugated Terpolymer Acceptors with Two Different Fused-Ring Electron-Deficient Building Blocks for Efficient All-Polymer Solar Cells. *ACS Appl. Mater. Interfaces* **2021**, *13*, 6442–6449.
- (27) Su, N.; Ma, R.; Li, G.; Liu, T.; Feng, L.-W.; Lin, C.; Chen, J.; Song, J.; Xiao, Y.; Qu, J.; Lu, X.; Sangwan, V. K.; Hersam, M. C.; Yan, H.; Facchetti, A.; Marks, T. J. High-Efficiency All-Polymer Solar Cells with Poly-Small-Molecule Acceptors Having  $\pi$ -Extended Units with Broad Near-IR Absorption. *ACS Energy Lett.* **2021**, *6*, 728–738.
- (28) Kim, J. S.; Lee, Y.; Lee, J. H.; Park, J. H.; Kim, J. K.; Cho, K. High-Efficiency Organic Solar Cells Based on End-Functional-Group-Modified Poly(3-hexylthiophene). *Adv. Mater.* **2010**, *22*, 1355–1360.
- (29) Park, J. K.; Jo, J.; Seo, J. H.; Moon, J. S.; Park, Y. D.; Lee, K.; Heeger, A. J.; Bazan, G. C. End-Capping Effect of a Narrow Bandgap Conjugated Polymer on Bulk Heterojunction Solar Cells. *Adv. Mater.* **2011**, *23*, 2430–2435.
- (30) Koldemir, U.; Puniredd, S. R.; Wagner, M.; Tongay, S.; McCarley, T. D.; Kamenov, G. D.; Müllen, K.; Pisula, W.; Reynolds, J. R. End Capping Does Matter: Enhanced Order and Charge Transport in Conjugated Donor–Acceptor Polymers. *Macromolecules* **2015**, *48*, 6369–6377.
- (31) Kim, S.; Park, J. K.; Park, Y. D. Charge transport behaviors of end-capped narrow band gap polymers in bottom-contact organic field-effect transistors. *RSC Adv.* **2014**, *4*, 39268–39272.

- (32) Zhang, Y.; Deng, J.; Mao, Q.; Young Jeong, S.; Huang, X.; Zhang, L.; Lee, B.; Huang, B.; Young Woo, H.; Yang, C.; Xu, J.; Wu, F.; Cao, Q.-Y.; Chen, L. Facilely full-end-capping engineering promotes high-performance organic solar cells with simultaneously improved efficiency and stability. *Chem. Eng. J.* **2023**, *457*, No. 141343.
- (33) Saxena, S.; Marlow, P.; Subbiah, J.; Colsmann, A.; Wong, W. W. H.; Jones, D. J. Pyridine End-Capped Polymer to Stabilize Organic Nanoparticle Dispersions for Solar Cell Fabrication through Reversible Pyridinium Salt Formation. *ACS Appl. Mater. Interfaces* **2021**, *13*, 36044–36052.
- (34) Giannopoulos, P.; Raptis, D.; Theodosiou, K.; Andreopoulou, A. K.; Anastasopoulos, C.; Dokouzis, A.; Leftheriotis, G.; Lianos, P.; Kallitsis, J. K. Organic dyes end-capped with perfluorophenyl anchors: Synthesis, electrochemical properties and assessment of sensitization capacity of titania photoanodes. *Dyes Pigm.* **2018**, *148*, 167–179.
- (35) Josse, P.; Dalinot, C.; Jiang, Y.; Dabos-Seignon, S.; Roncali, J.; Blanchard, P.; Cabanetos, C. Phthalimide end-capped thienoisindigo and diketopyrrolopyrrole as non-fullerene molecular acceptors for organic solar cells. *J. Mater. Chem. A* **2016**, *4*, 250–256.
- (36) Harris, J. D.; Carter, K. R. A one-pot strategy to improve end-capping efficacy in Stille poly-condensations. *Polym. Chem.* **2018**, *9*, 1132–1138.
- (37) Zheng, Q. D.; Jung, B. J.; Sun, J.; Katz, H. E. Ladder-Type Oligo-p-phenylene-Containing Copolymers with High Open-Circuit Voltages and Ambient Photovoltaic Activity. *J. Am. Chem. Soc.* **2010**, *132*, 5394–5404.
- (38) Wang, M.; Cai, D.; Yin, Z.; Chen, S.-C.; Du, C.-F.; Zheng, Q. Asymmetric-Indenothiophene-Based Copolymers for Bulk Heterojunction Solar Cells with 9.14% Efficiency. *Adv. Mater.* **2016**, *28*, 3359–3365.
- (39) Khan, F.; Dlugosch, M.; Liu, X.; Banwell, M. G. The Palladium-Catalyzed Ullmann Cross-Coupling Reaction: A Modern Variant on a Time-Honored Process. *Acc. Chem. Res.* **2018**, *51*, 1784–1795.
- (40) Hendriks, K. H.; Li, W.; Heintges, G. H. L.; van Puijzen, G. W. P.; Wienk, M. M.; Janssen, R. A. J. Homocoupling Defects in Diketopyrrolopyrrole-Based Copolymers and Their Effect on Photovoltaic Performance. *J. Am. Chem. Soc.* **2014**, *136*, 11128–11133.
- (41) Lombeck, F.; Komber, H.; Fazzi, D.; Nava, D.; Kuhlmann, J.; Stegerer, D.; Strassel, K.; Brandt, J.; de Zerío Mendaza, A. D.; Müller, C.; Thiel, W.; Caironi, M.; Friend, R.; Sommer, M. On the Effect of Prevalent Carbazole Homocoupling Defects on the Photovoltaic Performance of PCDTBT:PC71BM Solar Cells. *Adv. Energy Mater.* **2016**, *6*, No. 1601232.
- (42) Shi, M.; Wang, T.; Wu, Y.; Sun, R.; Wang, W.; Guo, J.; Wu, Q.; Yang, W.; Min, J. The Intrinsic Role of Molecular Mass and Polydispersity Index in High-Performance Non-Fullerene Polymer Solar Cells. *Adv. Energy Mater.* **2021**, *11*, No. 2002709.
- (43) Liu, Q.; Fang, J.; Wu, J.; Zhu, L.; Guo, X.; Liu, F.; Zhang, M. Tuning Aggregation Behavior of Polymer Donor via Molecular-Weight Control for Achieving 17.1% Efficiency Inverted Polymer Solar Cells. *Chin. J. Chem.* **2021**, *39*, 1941–1947.
- (44) Ding, Z.; Kettle, J.; Horie, M.; Chang, S. W.; Smith, G. C.; Shames, A. L.; Katz, E. A. Efficient solar cells are more stable: the impact of polymer molecular weight on performance of organic photovoltaics. *J. Mater. Chem. A* **2016**, *4*, 7274–7280.
- (45) Fan, B.; Ying, L.; Wang, Z.; He, B.; Jiang, X.; Huang, F.; Cao, Y. Optimisation of processing solvent and molecular weight for the production of green-solvent-processed all-polymer solar cells with power conversion efficiency over 9%. *Energy Environ. Sci.* **2017**, *10*, 1243–1251.
- (46) Shang, Z.; Zhou, L.; Sun, C.; Meng, L.; Lai, W.; Zhang, J.; Huang, W.; Li, Y. Non-equivalent D-A copolymerization strategy towards highly efficient polymer donor for polymer solar cells. *Sci. China: Chem.* **2021**, *64*, 1031–1038.
- (47) Oelmann, S.; Solleder, S. C.; Meier, M. A. R. Controlling molecular weight and polymer architecture during the Passerini three component step-growth polymerization. *Polym. Chem.* **2016**, *7*, 1857–1860.
- (48) Li, H. Q.; Yao, Y.; Wang, Z. M.; Cui, S. P.; Wang, Y. L. Influence of Monomer Ratios on Molecular Weight Properties and Dispersing Effectiveness in Polycarboxylate Superplasticizers. *Materials* **2020**, *13*, No. 1022.
- (49) Liu, P.; Dong, Z.; Kilbinger, A. F. M. Mono-telechelic polymers by catalytic living ring-opening metathesis polymerization with second-generation Hoveyda–Grubbs catalyst. *Mater. Chem. Front.* **2020**, *4*, 2791–2796.
- (50) Flory, P. J. *Principles of Polymer Chemistry*; Cornell University Press, 1953.
- (51) Stevens, M. P. *Polymer Chemistry*; Oxford University Press: New York, 1990.
- (52) Hiemenz, P. C.; Lodge, T. P. *Polymer Chemistry*; CRC Press, 2007.
- (53) Sivula, K.; Luscombe, C. K.; Thompson, B. C.; Fréchet, J. M. J. Enhancing the Thermal Stability of Polythiophene:Fullerene Solar Cells by Decreasing Effective Polymer Regioregularity. *J. Am. Chem. Soc.* **2006**, *128*, 13988–13989.
- (54) Carothers, W. H. Polymers and polyfunctionality. *Trans. Faraday Soc.* **1936**, *32*, 39–49.
- (55) Pirotte, G.; Kesters, J.; Cardeynals, T.; Verstappen, P.; D’Haen, J.; Lutsen, L.; Champagne, B.; Vanderzande, D.; Maes, W. The Impact of Acceptor-Acceptor Homocoupling on the Optoelectronic Properties and Photovoltaic Performance of PDTSQx(ff) Low Bandgap Polymers. *Macromol. Rapid Commun.* **2018**, *39*, No. 1800086.
- (56) Hong, W.; Chen, S. Y.; Sun, B.; Arnould, M. A.; Meng, Y. Z.; Li, Y. N. Is a polymer semiconductor having a “perfect” regular structure desirable for organic thin film transistors? *Chem. Sci.* **2015**, *6*, 3225–3235.
- (57) Dong, J.; Devi, P. S.; Sunil, D.; Mendoza, E.; Gafney, H. D. Photochemistry of Trimethyltin Iodide in Polar Media: Orbital Parentage and Observed Reactivity. *Inorg. Chem.* **2002**, *41*, 11–18.
- (58) Dhanabalan, A.; van Dongen, J. L. J.; van Duren, J. K. J.; Janssen, H. M.; van Hal, P. A.; Janssen, R. A. J. Synthesis, Characterization, and Electrooptical Properties of a New Alternating N-Dodecylpyrrole–Benzothiadiazole Copolymer. *Macromolecules* **2001**, *34*, 2495–2501.
- (59) Räder, H. J.; Spickermann, J.; Kreyenschmidt, M.; Mullen, K. MALDI-TOF mass spectrometry in polymer analytics. 2. Molecular weight analysis of rigid-rod polymers. *Macromol. Chem. Phys.* **1996**, *197*, 3285–3296.
- (60) Suárez, I.; Coto, B. Broadening of polymer chromatographic signals: Analysis, quantification and correction through effective diffusion coefficients. *J. Chromatogr. A* **2015**, *1407*, 193–202.
- (61) Baker, A. D.; Armen, G. H.; Funaro, S. Orbital levels of crown ethers and related macrocycles studied by ultraviolet photoelectron spectroscopy; relationship to complexation studies. *J. Chem. Soc., Dalton Trans.* **1983**, 2519–2523.
- (62) Vasil’ev, Y. V.; Khvostenko, O. G.; Streletskii, A. V.; Boltalina, O. V.; Kotsiris, S. G.; Drewello, T. Electron Transfer Reactivity in Matrix-Assisted Laser Desorption/Ionization (MALDI): Ionization Energy, Electron Affinity and Performance of the DCTB Matrix within the Thermochemical Framework. *J. Phys. Chem. A* **2006**, *110*, 5967–5972.
- (63) Wang, X.; Lu, H.; Liu, Y.; Zhang, A.; Yu, N.; Wang, H.; Li, S.; Zhou, Y.; Xu, X.; Tang, Z.; Bo, Z. Simple Nonfused Ring Electron Acceptors with 3D Network Packing Structure Boosting the Efficiency of Organic Solar Cells to 15.44%. *Adv. Energy Mater.* **2021**, *11*, No. 2102591.
- (64) Liu, X. Z.; Wei, Y. N.; Zhang, X.; Qin, L. Q.; Wei, Z. X.; Huang, H. An A-D-A'-D-A type unfused nonfullerene acceptor for organic solar cells with approaching 14% efficiency. *Sci. China: Chem.* **2021**, *64*, 228–231.
- (65) Xu, C. Y.; Jin, K.; Xiao, Z.; Zhao, Z. J.; Ma, X. L.; Wang, X. L.; Li, J. M.; Xu, W. J.; Zhang, S. P.; Ding, L. M.; Zhang, F. J. Wide Bandgap Polymer with Narrow Photon Harvesting in Visible Light Range Enables Efficient Semitransparent Organic Photovoltaics. *Adv. Funct. Mater.* **2021**, *31*, No. 2107934.

(66) Zhang, X.; Li, C. Q.; Qin, L. Q.; Chen, H.; Yu, J. W.; Wei, Y. N.; Liu, X. Z.; Zhang, J. Q.; Wei, Z. X.; Gao, F.; Peng, Q.; Huang, H. Side-Chain Engineering for Enhancing the Molecular Rigidity and Photovoltaic Performance of Noncovalently Fused-Ring Electron Acceptors. *Angew. Chem., Int. Ed.* **2021**, *60*, 17720–17725.

## Recommended by ACS

### Fused Benzotriazole A-Unit Constructs a D- $\pi$ -A Polymer Donor for Efficient Organic Photovoltaics

Zehua He, Erjun Zhou, *et al.*

JULY 28, 2023  
ACS MACRO LETTERS

READ 

### Design for a Pure-Blue-Emissive Polymer Film through the Selective Perturbation of the Energy Level of the Highest Occupied Molecular Orbital in a Boron Complex

Kazumasa Suenaga, Yoshiki Chujo, *et al.*

AUGUST 08, 2023  
MACROMOLECULES

READ 

### Double-Cable Conjugated Polymers Based on Simple Non-Fused Electron Acceptors for Single-Component Organic Solar Cells

Baiqiao Liu, Weiwei Li, *et al.*

JANUARY 26, 2023  
MACROMOLECULES

READ 

### Direct C–H Arylation-Derived Donor Polymers Afford PCEs over 10% for Organic Solar Cells

Ling-Jun Yang, Shi-Yong Liu, *et al.*

AUGUST 23, 2023  
ACS APPLIED POLYMER MATERIALS

READ 

Get More Suggestions >